ASTRONOMY & ASTROPHYSICS
SUPPLEMENT SERIES

Astron. Astrophys. Suppl. Ser. **125,** 303-312 (1997)

The Cepheus molecular cloud

I. Multi-transition observations in CO and ^{13}CO

G.P. Remy[1,2], I.A. Grenier[1,3,⋆], G. Duvert[4], and P. Thaddeus[5]

[1] EUROPA/Université Paris 7, Observatoire de Paris, Meudon, France
[2] Université de Cergy-Pontoise, Cergy-Pontoise, France
[3] CEA/DAPNIA/Service d'Astrophysique, Centre d'Études de Saclay, France
[4] Observatoire de Grenoble, St. Martin d'Hères, France
[5] Harvard-Smithsonian Center for Astrophysics, Cambridge, MA, U.S.A.

Received March 15, 1996; accepted January 10, 1997

Abstract. The eastern cloud of the nearby Cepheus complex, located at $111° < l < 117°$ and $14° < b < 19°$, has been mapped in the CO($J = 1 \rightarrow 0$) transition at a resolution of 0.8 pc with the CfA 1.2 m telescope. This massive, but fairly diffuse cloud, with visual extinction < 2 mag, has also been sampled in the $J = 1 \rightarrow 0$ and $2 \rightarrow 1$ rotational transitions of CO and ^{13}CO at the same resolution, using the CfA and POM-2 millimeter telescopes.

The radiative transfer of the lines has been treated in the LTE and LVG approximations, the two yielding comparable results. In CO, low excitation temperatures have been found in the range of $5 - 11$ K, with moderate optical depths ($\tau < 3$) and CO column-densities up to 4 10^{16} cm^{-2}. In ^{13}CO, the gas is optically thin with slightly lower excitation temperatures of $4 - 8$ K, for ^{13}CO column-densities up to 6 10^{15} cm^{-2}. Under these conditions, the observed ratios of $2 \rightarrow 1$ over $1 \rightarrow 0$ velocity-integrated intensities, $W_{2\rightarrow1}/W_{1\rightarrow0}$, have been found to be consistent with a uniform value over the cloud of 0.88 ± 0.09 in CO and 0.60 ± 0.07 in ^{13}CO, as typical of many clouds.

The ratios of CO over ^{13}CO velocity-integrated intensities, $W(^{12}\mathrm{CO})/W(^{13}\mathrm{CO})$, have been found to decrease with ^{13}CO intensity as expected from the progressive saturation of the CO lines. The large scatter about this relation, observed at scales of 0.8 and 0.2 pc, cannot be accounted for by instrumental error, beam dilution, or the dispersion of excitation temperatures and line widths measured in the cloud. The $W(^{12}\mathrm{CO})/W(^{13}\mathrm{CO})$ fluctuations are therefore indicative of intrinsic variations in the molecular abundances. In particular, very low $W(^{12}\mathrm{CO})/W(^{13}\mathrm{CO})$ ratios may result from efficient isotopic fractionation in this cold environment. Similar variations in ^{13}CO intensity have been reported at a scale of 0.2 pc in two other dark clouds, HCL 2 (Cernicharo & Guélin 1987) and IC 5146 (Lada et al. 1994), from the behaviour of their $W(^{12}\mathrm{CO})/W(^{13}\mathrm{CO})$ or $W(^{13}\mathrm{CO})/A_V$ ratios with visual extinction. Together with the present results, they suggest that the ^{13}CO abundance integrated along the line of sight largely varies inside the diffuse envelopes of molecular clouds.

Key words: ISM: Cepheus cloud — ISM: abundances — ISM: clouds — ISM: molecules — radio lines: ISM

1. Introduction

Mapped in CO at a resolution of 0.5° by Lebrun (1986) and Grenier et al. (1989), the Cepheus Flare region contains a massive molecular complex at an estimated distance of $\sim$ 300 pc. The complex lies high above the Galactic plane, at a displacement $z \sim 90$ pc. A recent re-evaluation of the $N(\mathrm{H_2})/W(\mathrm{CO})$ conversion factor in nearby clouds (Digel et al. 1996) brings its total H_2 mass down to 3 10^4 solar masses, equivalent to Orion B and slightly less than Orion A (4 10^4 $M_\odot$). It is comparable in size to the Orion and Taurus complexes, but it contains no massive star or HII region and exhibits surprisingly little star formation. Extinction through the cloud does not exceed 2 mag (Lebrun 1986). It is therefore apparently a rather massive, but cold and diffuse, molecular object, intermediate between the dense, active star-forming clouds near the Galactic plane and the translucent, light ones at high latitude.

Because of its large angular size, the complex had been first surveyed in CO at a resolution so low that only limited information as to its internal structure could be

Send offprint requests to: I.A. Grenier
⋆ Service d'Astrophysique, Centre d'Études de Saclay, 91191 Gif/Yvette, France.

obtained. To study this structure better, though on a limited scale, we chose the brightest cloud of the complex, located near the eastern border at $l = 111° - 117°$ and $b = 14° - 19°$, to be fully mapped in the CO($1 \rightarrow 0$) line at an angular resolution of $8.7'$, i.e. approximately 0.8 pc at 300 pc. This elongated cloud, which we will refer to as the "eastern cloud", spans a region of 10 by 20 pc. The IRAS source $22343+7501$, embedded in the southern tip of the cloud, has been associated with a 1 or 2 pc-long bipolar outflow, observed in CO and ^{13}CO by Sato & Fukui (1989). No other infrared source has been found in the cloud except IRAS $22376+7455$ a little beyond the southern edge. With no massive star, the cloud is almost free of internal source of radiative heating.

To determine the gas characteristics, a multi-transition CO analysis has been undertaken and observations have been carried out at the same resolution in the $J = 1 \rightarrow 0$ and $2 \rightarrow 1$ transitions of CO and ^{13}CO. The weakness of the ^{13}CO emission and the extent of the cloud prevented us from mapping it at all frequencies; instead, a set of positions has been selected as representative of the entire cloud, spanning both the brightness-temperature range and velocity structure.

The eastern cloud has also been chosen because it exhibited unusually wide CO lines in the low-resolution survey (Grenier et al. 1989). The higher resolution data show that the broad lines result from the superposition of two or three lines of normal width which drift in velocity across the cloud according to a peculiar, highly organized velocity field. The hydrodynamical study of this field, indicative of a slow, large-scale flow that stirs the cloud and spreads the line velocities between -8 and $+2$ km/s, will be presented in a following paper (Paper III). For the present purpose, the composite lines have been fitted by two or three gaussian profiles, which have then been treated as independent components of the cloud emission.

Surveys at comparable resolution of the Cepheus Flare region exist at various wavelengths, from radio to γ rays, to map its gas and dust content; the different tracers of molecular gas may therefore be compared in a single cloud. This will be done in Paper II, using column-densities derived from the present multi-transition study.

The following sections will describe the observations, determinations of the transition and isotopic line ratios and their variations over the cloud, and the derivation of the excitation conditions of the CO and ^{13}CO molecules under LTE and LVG assumptions.

2. Observations

2.1. $J = 1 \rightarrow 0$ *transitions*

The CO and ^{13}CO observations of the $J = 1 \rightarrow 0$ transitions at 115 and 110 GHz, respectively, have been carried out in March and April 1991 with the Center for Astrophysics (CfA) 1.2 m telescope in Cambridge, Massachusetts. The full beam size at half maximum is $8.7'$ at 115 GHz. 1407 CO spectra, spaced every $0.125°$ along a regular (l, b) coordinate grid, cover a total of 22 deg^2. A set of positions has been subsequently selected to sample the cloud in ^{13}CO, covering the whole range of observed peak temperatures and line velocities (see Fig. 1).

The receiver is a sensitive liquid helium-cooled SIS mixer, with a typical single-sideband noise temperature of about 65 K at the time of the observations. Spectral resolution is provided by a 256-channel filter-bank spectrometer. We used a frequency resolution of 250 kHz, i.e. a velocity resolution of 0.65 and 0.68 km/s at 115 and 110 GHz, respectively, centered on 0 km/s in the local standard of rest. Because of telluric CO emission at velocities close to the range of interest and because of the large width of the expected lines, all spectra have been observed in position-switching mode using two reference positions to straddle the source in elevation. The latter positions have been checked by frequency switching to be free of appreciable CO emission. Position switching was also preferred because it yields very flat spectral baselines that generally allow a clear decomposition of the multiple lines into gaussian components. Only linear baselines have been removed from the raw spectra. For overall system temperatures including the atmosphere of $400-800$ K in CO and $300-400$ K in ^{13}CO, typical integration times of at most a few minutes were needed to achieve a rms noise of 0.1 K in radiation temperature.

Calibration and correction for atmospheric absorption have been made by briefly rotating a room-temperature blackbody wheel in front of the feed horn before each scan. The temperature and opacity of atmospheric water vapor have been estimated by antenna tipping as often as weather variations required. To check the pointing and calibration, a reference position has been repeatedly observed in Cepheus; day-to-day intensity variations amount to 4%. *The resulting radiation temperatures have been scaled by a factor of 1.22 to correct them to absolute brightness temperatures* as recommended by Bronfman et al. (1988) after their re-evaluation of the beam efficiency.

2.2. $J = 2 \rightarrow 1$ *transitions*

The higher-frequency transition of CO and ^{13}CO have been observed during the winters of 1994 and 1995 with the POM-2 2.5 m telescope on the Plateau de Bure in France. The beam size at half intensity of the antenna is $2'.3$ at 230 GHz. The telescope is equipped with an SIS receiver, cooled by a 2 K cryogenerator, and a 256-channel autocorrelator back-end. The CO and ^{13}CO data, at 230 and 220 GHz, respectively, have been taken with a 312 kHz resolution that corresponds to velocity resolutions of 0.41 and 0.43 km/s. As for the CfA telescope, the back-end was centered on 0 km/s in the local standard of rest. In order to reduce the integration time, and because the telluric CO line lay more than 5 km/s away from those

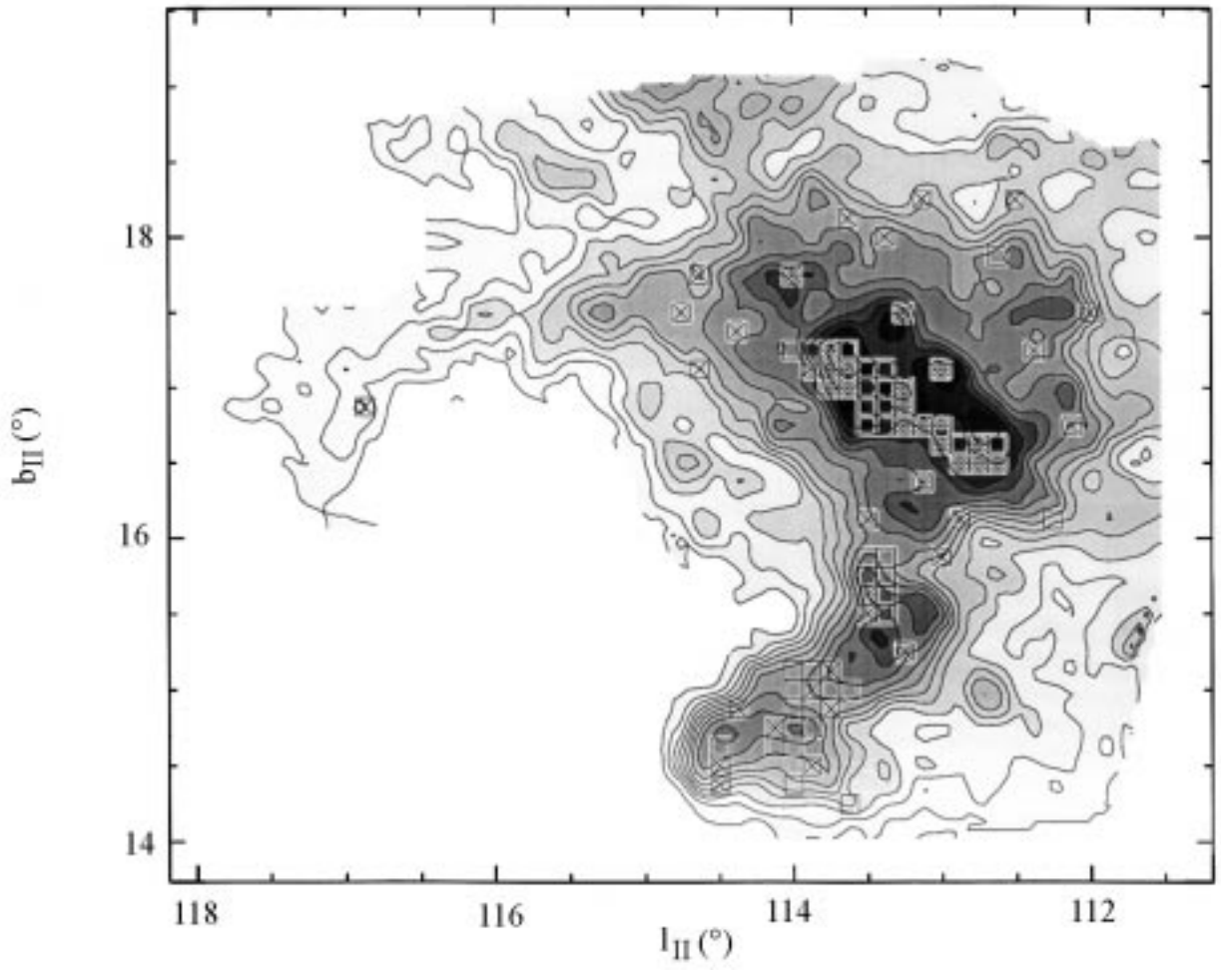

Fig. 1. Map of the CO emission at 115 GHz, integrated between −10 and +10 km/s in radial velocity, from the eastern cloud of the Cepheus complex. The angular resolution is 8.7′. Contours increase from 1.3 K km/s (3σ) with a step of 2 K km/s. The positions sampled at 110, 220 GHz (x) and 230 GHz (□) have been superimposed

of interest, frequency switching has been adopted, with a switching interval of 18 MHz.

To allow a comparison of the $2 \rightarrow 1$ and $1 \rightarrow 0$ spectra, the POM-2 data have been smoothed to the CfA beam resolution. To do so, each selected position observed in $1 \rightarrow 0$ has been mapped in $2 \rightarrow 1$; the map, centered on the position of the $1 \rightarrow 0$ spectrum, consists of 4 by 4 positions spaced every 2′ along a regular (l, b) coordinate grid. After folding the raw spectra, each map has been convolved with the CfA antenna pattern. To achieve an rms noise of 0.05 K on the synthesized spectra, individual scans have been integrated to a noise level lower than 0.4 K. For system temperatures of 500 to 1500 K for both lines, typical integrations were 2 min per spectrum. As a final step, baselines of order 3 to 5 have been subtracted from the synthesized spectra. The POM-2 radiation temperature scale has been corrected for the main beam efficiency and for atmospheric absorption by means of ambient hot-cold calibration blackbodies at the telescope and a standard atmospheric model (Kutner 1978). Pointing and calibration have been tested in Orion at the beginning of each observing run and on the reference position in Cepheus every hour. Observed intensity variations were no more than 7%. *The radiation temperatures have been scaled by a factor of 1.3 to match the expected intensity from the Orion reference position*. The calibration of POM-2 has been checked against the AT&T Bell Laboratories 7 m telescope using the Barnard 5 source to study multi CO transitions in Orion A (Castets et al. 1990).

3. Results and discussion

Contours of the observed CO($1 \rightarrow 0$) line intensities, $W_{1\rightarrow0}$(CO), integrated between −10 and +10 km/s in velocity are presented in Fig. 1. The lowest contour lies 3 times above the noise level. The structure of the cloud, with a sharp eastern edge, a diffuse boundary on the west, and a comet-like extension to the south, confirms the main

features that had been seen in the low-resolution survey. The present higher resolution does not reveal much more structure in the interior. The few apparent clumps mainly result from velocity crowding along the line of sight.

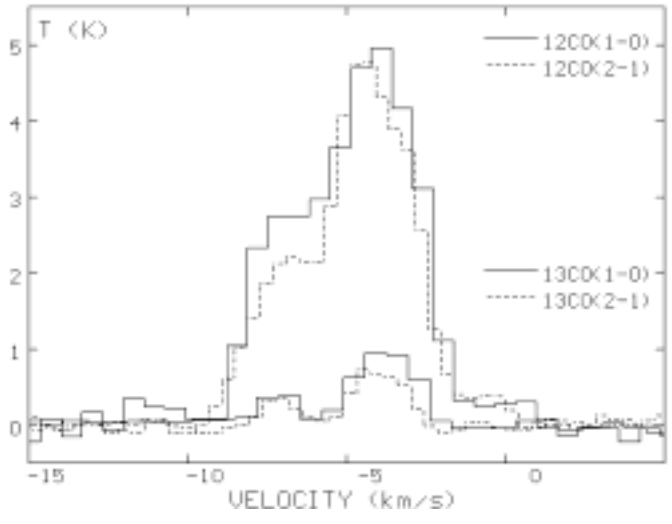

Fig. 2. Example of composite lines recorded in the eastern cloud in CO($1 \rightarrow 0$), CO($2 \rightarrow 1$), ^{13}CO($1 \rightarrow 0$), and ^{13}CO($2 \rightarrow 1$) from more to less intense lines

The various positions observed at 110, 220, and 230 GHz are indicated in Fig. 1. Other positions have been sampled along the fainter edges of the cloud, but they lacked of ^{13}CO emission at the achieved sensitivity. An example of bright composite lines observed in the cloud is given in Fig. 2 for both transitions and both isotopes. The multiple lines have been fitted by two gaussian profiles, sometimes three. The central velocity of each component has been checked to coincide in the four transitions. The line widths of $\sim$ 3 km/s in CO and $\sim$ 2 km/s in ^{13}CO found for the gaussians agree with those of the single lines found elsewhere in the cloud. Each component has then been analysed separately.

To study line ratios, the weak detections have been discarded and only lines with an integrated intensity greater than 2σ have been retained. This threshold is slightly lower than the customary 3σ level since the presence of a line at the same velocity at all four frequencies reinforces its detection probability in a single spectrum. Hence, sets of 60 to 120 lines were prepared to compare emission at two frequencies, all at the same angular resolution of $8.7'$ or 0.8 pc at 300 pc. Integrated intensities rather than peak temperatures have been selected to study the line ratios because of their smaller uncertainty. The observed diffuseness of the cloud on scales larger than the angular resolution should limit the beam dilution effects on the derived line ratios. This point is confirmed by the limited ($< 20\%$) intensity variations recorded among the individual $2.3'$ POM-2 scans contained within one CfA beam.

3.1. Line-ratio determination

The average line ratio over the cloud has not been derived, as is often done, by taking the mean or weighted mean of the individual line ratios, because these estimates are *strongly biased* - in the present case towards low values. We studied instead the correlation between the velocity integrated intensities measured at the $2 \rightarrow 1$ and $1 \rightarrow 0$ frequencies, noted $W_{2\rightarrow1}$ and $W_{1\rightarrow0}$, respectively. We did not attempt linear least-square fits to the data since the relative uncertainties on the points are comparable on both axes. Linear fits have been obtained instead by adopting a maximum-likelihood analysis that takes uncertainties on both axes into account. Assuming gaussian distributions, the log-likelihood function to optimize is written as:

$$L(a, b, \mu_i) = -\frac{1}{2} \sum_{\text{all points}} \frac{(y_i - a - b\mu_i)^2}{\sigma_{y_i}^2} + \frac{(x_i - \mu_i)}{\sigma_{x_i}^2} \quad (1)$$

where (x_i, y_i) represent the observed point coordinates with instrumental uncertainties σ_{xi} and σ_{yi}, and a and b characterize the linear function to be fitted together with the parent population of points (μ_i, $a + b\mu_i$) that is compatible with the given linear regression. The likelihood function is therefore maximized over $N + 2$ free parameters, N being the number of parent or observed points. The consistency between the observed points and their likeliest parent counterpart is used to check the relevance of the proposed fit. Statistical errors on a, b, and μ_i have been derived from the information matrix (Strong 1985); quoted errors are 1σ.

3.2. $W_{2\rightarrow1}/W_{1\rightarrow0}$ ratios

Figures 3a and 3b illustrate the tight correlation that exists between the $2 \rightarrow 1$ and $1 \rightarrow 0$ velocity-integrated intensities for the two isotopic species of CO we have observed. The small scatter implies that the $W_{2\rightarrow1}/W_{1\rightarrow0}$ ratio is fairly uniform in the emitting regions and independent of the CO brightness. Linear fits to the points give:

$$W_{2\rightarrow1}(\text{CO}) = (0.88 \pm 0.02)\ W_{1\rightarrow0}(\text{CO}) - (0.84 \pm 0.16)$$

$$W_{2\rightarrow1}(^{13}\text{CO}) = (0.60 \pm 0.02)\ W_{1\rightarrow0}(^{13}\text{CO}) + (0.0 \pm 0.03).$$

The intercepts are consistent with zero given the instrumental sensitivity. The statistical error on the slopes takes into account the noise level in each spectrum and the $\pm4\%$ or $\pm7\%$ uncertainty from day-to-day variations in the calibration of each telescope. In addition, the derived line ratios suffer from a $\pm10\%$ systematic uncertainty in the absolute calibration of each telescope which reduces the accuracy of the integrated intensities significantly. Hence the transition ratios are

in CO: $W_{2\rightarrow1}/W_{1\rightarrow0} = 0.88 \pm 0.09$

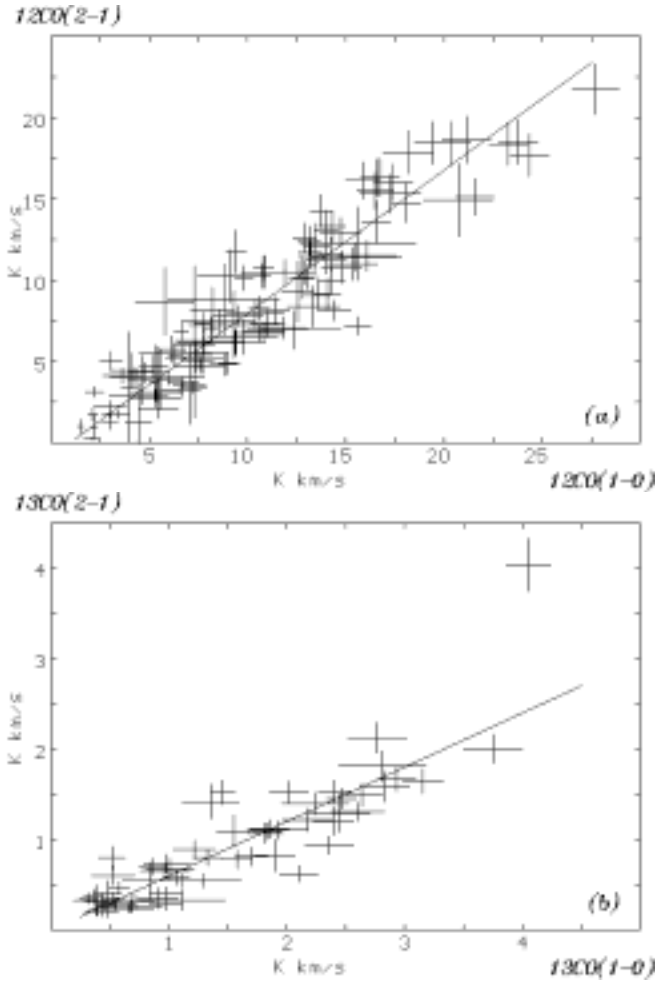

Fig. 3. Correlations between velocity-integrated CO intensities observed in the $2 \rightarrow 1$ and $1 \rightarrow 0$ transitions, $W_{2\rightarrow1}$ versus $W_{1\rightarrow0}$, for CO **a)** and ^{13}CO **b)**. The fitted slopes are 0.88 ± 0.02 and 0.60 ± 0.02, respectively

in ^{13}CO: $W_{2\rightarrow1}/W_{1\rightarrow0} = 0.60 \pm 0.07$.

Because the line widths in both transitions are always nearly equal (see Fig. 2), the ratios of $2 \rightarrow 1$ over $1 \rightarrow 0$ peak temperatures have the same average values.

In CO, the mean $W_{2\rightarrow1}/W_{1\rightarrow0}$ ratio agrees with those measured in clouds of various types. For the giant molecular clouds in the Galactic plane, Sanders et al. (1993) find a ratio at the solar circle of $0.9 - 0.95$ and an average in the inner Galaxy of 0.8 ± 0.1, varying little with galactocentric distance. In nearby, dense globules such as HCL 2 in Taurus, or B157 and L1075 in Cygnus, ratios of 1.2 ± 0.2 and 0.77 ± 0.15 have been found by Cernicharo & Guélin (1987) and Robert & Pagani (1993), respectively. Van Dishoeck et al. (1991) have derived an average ratio of 0.77 ± 0.21 for both high-latitude clouds and translucent ones of visual extinction equivalent to that of Cepheus (< 2 or 3 mag). The apparent stability of these ratios has theoretical grounds: in plane-parallel models of clouds with uniform density and illuminated by the interstellar radiation field (Lequeux et al. 1994, and references therein), the emergent $W_{2\rightarrow1}/W_{1\rightarrow0}$ ratio increases with cloud density from 10^3 to 10^5 cm^{-3}, but by less than a factor of 2. The weakness of this dependence on density results from line saturation and decreasing gas temperature. This dependence may have been observed by Sakamoto et al. (1994) in the Orion complex where the $W_{2\rightarrow1}/W_{1\rightarrow0}$ ratios increase from 0.5 near the cloud edges to ~ 1 in the bright, optically thick, central ridge, around mean values of 0.77 and 0.66 in Orion A and B, respectively. The Cepheus cloud is not bright enough to show this effect since the $W_{2\rightarrow1}/W_{1\rightarrow0}$ ratios in our sample do not depend on CO brightness up to 30 K km/s (see Fig. 3a).

In ^{13}CO, the $W_{2\rightarrow1}/W_{1\rightarrow0}$ ratio in Cepheus agrees with those determined in the B157 and L1075 globules (0.58 ± 0.18, Robert & Pagani 1993) and in a high-latitude clump, MCLD126.6 + 24.6 of the Polaris complex (0.45 ± 0.06, Boden & Heithausen 1993). The more emissive HCL 2 globule, which exhibits saturated ^{13}CO lines, gives line ratios close to 1.0 ± 0.2 (Cernicharo & Guélin 1987). In Cepheus, the ratio peaks near unity in the denser clump of gas surrounding the IRAS source, where the optical depth in ^{13}CO is close to unity.

3.3. Excitation temperatures, opacities, and column-densities

The radiation temperature $T^*(\nu)$ of a line at frequency ν, arising from a cloud of optical depth $\tau(\nu)$ filling the telescope beam, is given for an excitation temperature $T_{\rm ex}$ by:

$$T^* = \frac{h\nu}{k}(1 - \mathrm{e}^{-\tau(\nu)}) \left(\frac{1}{\mathrm{e}^{\frac{h\nu}{kT_{\rm ex}}} - 1} - \frac{1}{\mathrm{e}^{\frac{h\nu}{k(2.7\mathrm{K})}} - 1} \right). \qquad (2)$$

Under conditions of local thermodynamic equilibrium (LTE), assuming identical excitation temperatures for both transitions, as suggested by the rather uniform $W_{2\rightarrow1}/W_{1\rightarrow0}$ ratios and the low brightness temperatures recorded, the ratio of the optical depths in the two transitions is expressed below with $\Delta\nu$ representing the line width in frequency:

$$\frac{\tau_{2-1}}{\tau_{1-0}} = 4 \left(\frac{1 - \mathrm{e}^{-\frac{2h\nu_{1-0}}{kT_{\rm ex}}}}{\mathrm{e}^{\frac{h\nu_{1-0}}{kT_{\rm ex}}} - 1} \right) \frac{\Delta\nu_{1-0}}{\Delta\nu_{2-1}}. \qquad (3)$$

In order to derive the excitation temperature, optical depth and related column-density of the emitting gas for each line, observed velocity-integrated intensities have been preferred to peak radiation temperatures for statistical reasons. The equations $\int T^*_{1-0}(\nu)\ \mathrm{d}\nu = W_{1\rightarrow0}$ and $\int T^*_{2-1}(\nu)\ \mathrm{d}\nu = W_{2\rightarrow1}$ have been solved numerically in $T_{\rm ex}$ and $\tau_{1\rightarrow0}$ for the observed intensities $W_{1\rightarrow0}$ and $W_{2\rightarrow1}$ of a line, assuming for the integration a gaussian

Table 1. Results from the LTE transfer and the LVG model for different kinetic temperatures: number of lines used, $N_{\rm tot}$, and admitting a solution, $N_{\rm sol}$, mean excitation temperatures, $T_{\rm ex1-0}$ and $T_{\rm ex2-1}$ in K, and mean optical depths, τ_{1-0} and τ_{2-1}, in the two transitions, column-densities, N in 10^{15} cm^{-2}, for each CO isotope, and H_2 volume densities, $n(H_2)$ in 10^3 cm^{-3}. The quoted errors represent the rms dispersion of the distributions

	LTE	LVG			
		8 K	10 K	15 K	30 K
CO					
$N_{\rm tot}$	116	116	116	116	116
$N_{\rm sol}$	115	61	109	114	112
$T_{\rm ex1-0}$	7.0±1.4	7.9±0.2	9.8±0.5	13.8±1.8	20.9±7.2
$T_{\rm ex2-1}$	7.0±1.4	7.0±0.7	8.2±1.1	8.8±1.5	9.1±1.7
τ_{1-0}	1.7±1.2	0.8±0.4	0.7±0.4	0.4±0.2	0.2±0.1
τ_{2-1}	2.3±1.4	1.3±0.7	1.4±0.7	1.1±0.4	1.0±0.3
N(CO)	17.7±12.3	9.9±6.8	12.3±8.5	9.3±5.6	8.3±4.6
$n(H_2)$		48^{+96}_{-48}	18^{+21}_{-18}	4.4±2.2	1.7±0.6
^{13}CO					
$N_{\rm tot}$	60	46	46	46	46
$N_{\rm sol}$	59	45	46	46	45
$T_{\rm ex1-0}$	5.2±1.2	7.5±0.8	8.7±1.5	10.7±3.3	13.5±8.3
$T_{\rm ex2-1}$	5.2±1.2	5.7±0.9	5.9±1.1	6.1±1.3	6.1±1.3
τ_{1-0}	0.5±0.3	0.2±0.1	0.1±0.1	0.1±0.1	0.1±0.1
τ_{2-1}	0.5±0.4	0.3±0.2	0.2±0.2	0.2±0.1	0.2±0.1
$N(^{13}$CO)	2.3±1.6	1.1±0.9	1.0±0.7	1.0±0.7	0.9±0.6
$n(H_2)$		14^{+22}_{-14}	6^{+8}_{-6}	2.2±1.5	0.9±0.5

profile for $\tau(\nu)$ with $\Delta\nu$ equal to the observed width of the line. Molecular column-densities have then been calculated in the LTE approximation. CO and ^{13}CO emission have been treated independently. Histograms of the excitation temperatures, $(1 \rightarrow 0)$ optical depths, and column-densities found in the cloud are displayed in Fig. 4. The mean and rms dispersion of these distributions are given in Table 1. The data in Fig. 4b imply optically thin conditions in ^{13}CO and moderate optical depths in CO ($\tau_{1\rightarrow0} < 3$ typically). The optical depths in the higher transition are less than twice higher. These low optical depths and the narrow temperature distributions do explain the uniform $W_{2\rightarrow1}/W_{1\rightarrow0}$ ratios found in the cloud. Indeed, Eq. (3) in the optically thin regime and values of $W_{2\rightarrow1}/W_{1\rightarrow0} = 0.88 \pm 0.09$ (in CO) and 0.60 ± 0.07 (in ^{13}CO) yield excitation temperatures of (6.7 ± 0.5) K and (5.0 ± 0.3) K, respectively, which are totally consistent with the temperature distributions displayed in Fig. 4a that have a mean and rms dispersion of (7.0 ± 1.4) K in CO and (5.2 ± 1.2) K in ^{13}CO.

The radiative transfer equation is considerably simplified for systematic motions of the gas (Sobolev 1960; Castor 1970). The so-called "large velocity gradient" models provide numerical solutions for a constant velocity gradient under the assumptions of statistical equilibrium and a complete photon redistribution in frequency and angle. Far from being randomly distributed, the velocity field in this cloud appears to be highly organized and presents large gradients of amplitude 0.4 km s^{-1} pc^{-1} (Paper III), unfortunately measured perpendicularly to the line-of-sight. However, their presence gives support to the LVG approximation and to the model which treats line formation at different locations independently. We have used the model developed by Castets et al. (1990). Its numerical simplicity allows conversion of line intensities to volume gas density and molecular column-density, given the local kinetic temperature, $T_{\rm k}$, and two line transitions. Various kinetic temperatures from 8 to 30 K have been tested. The choice of collision rates (from Green & Thaddeus 1976 or Flower & Launay 1985) and the geometry of the cloud (spherical or plane parallel) has little influence on the inferred characteristics of the gas. Histograms of the $(2 \rightarrow 1)$ excitation temperatures, $(1 \rightarrow 0)$ optical depths, and column-densities found in the cloud in CO and ^{13}CO

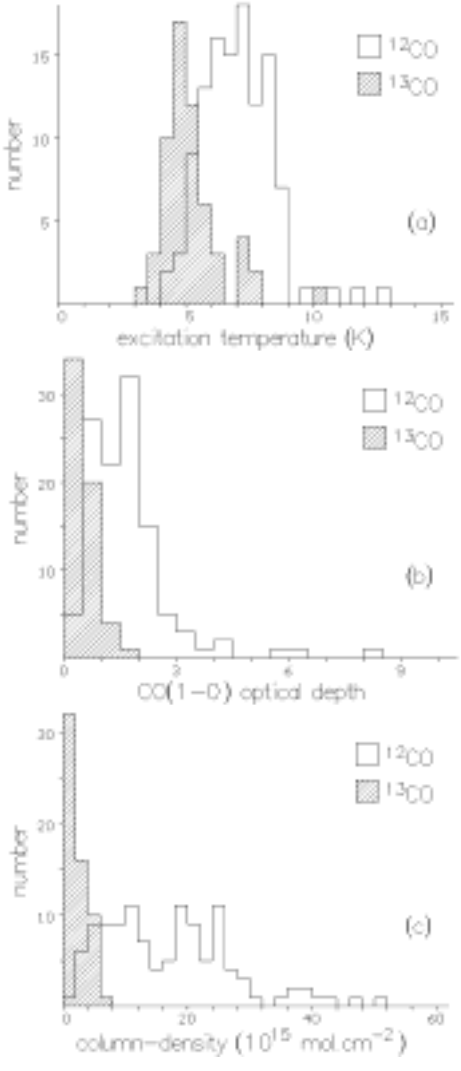

Fig. 4. Number distributions of the excitation temperatures **a)**, optical depths in the $1 \rightarrow 0$ transition **b)**, and molecular column-densities **c)**, derived in the LTE approximation from the observed CO and ^{13}CO lines

are displayed in Fig. 5. The mean and rms dispersion of these distributions are also given in Table 1. The choice of kinetic temperature has little influence on these distributions. On the contrary, the volume densities and the $1 \rightarrow 0$ excitation temperatures are not constrained by the models. Kinetic temperatures below 8 K could not be tested because the adopted collision rates did not apply. At $T_{\rm k} = 8$ K, the LVG model still finds a solution for half of the CO sample and all the ^{13}CO sample. The narrow distributions displayed in Fig. 5 nicely corroborate the LTE findings. The moderate $1 \rightarrow 0$ optical depths ($\tau_{1\rightarrow0} < 2$) are even lower than the LTE estimates. The small (not significant) discrepancy between the cloud average ($2 \rightarrow 1$) temperatures found in the LTE and LVG models may be due to our limitation in $T_{\rm k} > 8$ K.

The consistent LTE and LVG results therefore yield excitation temperatures in the cloud in the range of $5-11$ K in CO and $4-8$ K in ^{13}CO. These low values indicate little heating by the external UV field - perhaps as the result of the high elevation of Cepheus above the Galactic plane (90 pc) and the lack of massive stars in its interior or vicinity. The small range of excitation temperatures and uniform $W_{2\rightarrow1}/W_{1\rightarrow0}$ ratios apply to column-densities below typically a few 10^{16} molecules cm^{-2} (Figs. 4c, 5e, and 5f). The cloud is moderately thick in CO and optically thin in ^{13}CO. These rather "transparent" conditions justify the close excitation temperatures found in CO and ^{13}CO. In denser, brighter clouds such as Orion A, larger differences have been found because the saturated lines of both isotopes probe regions of distinct density (Castets et al. 1990). In HCL 2 for instance (Cernicharo & Guélin 1987), CO, ^{13}CO, and C^{18}O are detected at extinctions above 0.5, 0.7, and 1.5 mag, respectively, which correspond to differences in temperature of several Kelvin according to the model of Lequeux et al. (1994).

3.4. $W(^{12}CO)/W(^{13}CO)$ ratios

Figures 6a and 6b compare the velocity-integrated intensities recorded from the ^{12}CO and ^{13}CO isotopes. They reveal significant fluctuations of the $W(^{12}\mathrm{CO})/W(^{13}\mathrm{CO})$ ratios from point to point for both line transitions. While being less sensitive to the absolute calibration of the telescopes, the $W(^{12}\mathrm{CO})/W(^{13}\mathrm{CO})$ ratios depend more on the signal-to-noise ratio of the weaker ^{13}CO detections and on the day-to-day variations in the calibration. With these uncertainties, linear fits have been applied to the data in Fig. 6 according to the method described in Sect. 3.1. They yield averages of the $W(^{12}\mathrm{CO})/W(^{13}\mathrm{CO})$ ratios over the cloud of 7.1 ± 0.5 and 10.0 ± 1.0 for the $1 \rightarrow 0$ and $2 \rightarrow 1$ transitions, respectively. The highly dispersed points are clearly not consistent with these means.

Figures 7 and 8 demonstrate that the $W(^{12}\mathrm{CO})/W(^{13}\mathrm{CO})$ ratios decrease with the velocity-integrated ^{13}CO intensity, $W(^{13}\mathrm{CO})$, in a similar way for the $1 \rightarrow 0$ and $2 \rightarrow 1$ transitions. The high ratios recorded at low intensity cannot be attributed to a finite instrumental sensitivity or a poor signal-to-noise ratio in the ^{13}CO spectra since only firm detections have been retained in these figures. The apparent decrease of the ratios with $W(^{13}\mathrm{CO})$ can be explained by the rapid saturation of the bright CO lines as shown in Figs. 7 and 8: the solid line indicates the change in $W(^{12}\mathrm{CO})/W(^{13}\mathrm{CO})$ with increasing ^{13}CO column-density as predicted by the radiative transfer of CO lines treated under LTE assumptions. A standard isotopic ratio [CO]/[^{13}CO] of 77 ± 7 (Wilson & Rood 1994) has been used to produce this curve, together with an excitation temperature in CO and in ^{13}CO equal to the mean values derived above (7.0 K and 5.2 K, respectively). To follow the increase in optical depth and the progressive saturation of the line core, line

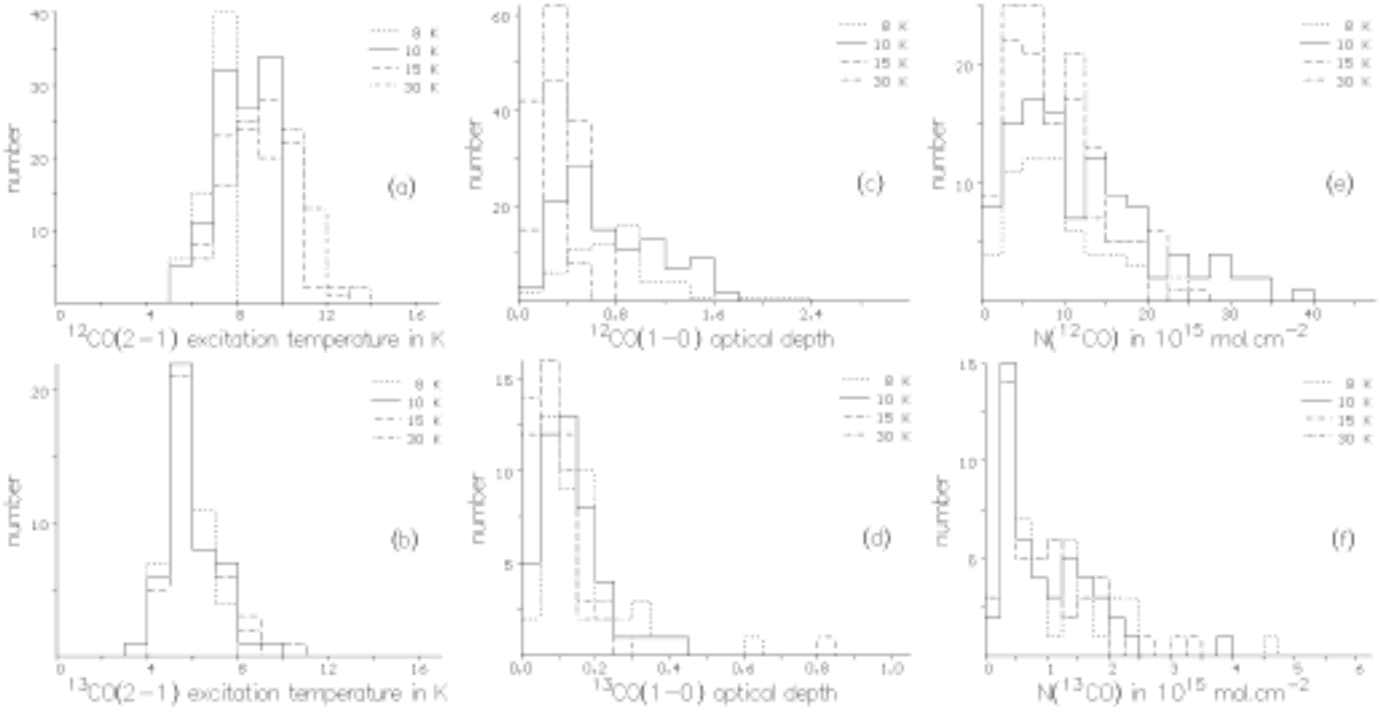

Fig. 5. Number distributions of the excitation temperatures in CO($2 \rightarrow 1$) **a)** and ^{13}CO($2 \rightarrow 1$) **b)**, of the optical depths in CO($1 \rightarrow 0$) **c)** and ^{13}CO($1 \rightarrow 0$) **d)**, and of the column-densities in CO **e)** and ^{13}CO **f)**, derived from the observed lines and the LVG model for kinetic temperatures between 8 and 30 K

integrals $\int T^*(V)\ \mathrm{d}V$ of the CO and ^{13}CO radiation temperatures have been calculated for increasing ^{13}CO column-density, assuming a gaussian velocity profile with a full-width to half-maximum (FWHM) ΔV of ~ 2 km/s, typical of the optically thin ^{13}CO lines detected in the cloud. Calculations have been conducted for both transitions. The resulting curves in Figs. 7 and 8 nicely agree with the envelope of the data points. The high ratios obtained at low $W(^{13}\mathrm{CO})$ arise from optically thin conditions for both isotopic species. The asymptotic value of ~ 3 measured at large $W(^{13}\mathrm{CO})$, when ^{13}CO line cores become optically thick, is commonly reached in other dense globules of high optical depth: $\sim$ 3 in B157 and L1075 (Robert & Pagani 1993), 2.7 ± 0.9 in MCLD $126.6 + 24.5$ (Boden & Heithausen 1993), ~ 2.5 in HCL2 (Cernicharo & Guélin 1987).

In addition to the overall decrease in $W(^{12}\mathrm{CO})/W(^{13}\mathrm{CO})$ as a function of $W(^{13}\mathrm{CO})$, a large dispersion in the ratios about this relation can be seen in Figs. 7 and 8. The significant fluctuations have been recorded in the two transitions and by two different telescopes. The same behaviour has been reported in two other clouds. In HCL 2, Cernicharo & Guélin (1987) have observed highly dispersed $W(^{12}\mathrm{CO})/W(^{13}\mathrm{CO})$ ratios, decreasing as a function of visual extinction A_V between 1 and 7 mag, as derived from star counts. The amplitude of the fluctuations on a 0.2 pc scale is equivalent to that in Cepheus. Using more precise extinction measurements from near-infrared star observations toward the dark cloud IC 5146, Lada et al. (1994) have found that the ratios of ^{13}CO column-density to A_V, $N(^{13}\mathrm{CO})/A_V$, present large fluctuations at low A_V and the ratios decrease with increasing A_V up to 30 mag, probably because of the saturation of the ^{13}CO lines. They argue that the large dispersion at low A_V is not caused by the instrument, nor by the scatter in the extinction measurements. The fluctuations have a larger amplitude on a 0.2 pc scale than in Cepheus. Hence, data from HCL 2, IC 5146, and Cepheus suggest that large intrinsic fluctuations in the ^{13}CO abundance or its excitation conditions occur in the outer layers of some molecular clouds. Similar conclusions have been reached by Langer et al. (1989) studying the $W(^{13}\mathrm{CO})/W(\mathrm{C}^{18}\mathrm{O})$ ratio in Barnard 5. The fluctuations appear at A_V below ~ 1 mag in Cepheus, ~ 2 mag in HCL 2 and ~ 3 mag in IC 5146.

The height of the LTE model curve in Figs. 7 and 8 is determined by the excitation temperature T_{ex}(CO) in CO, the FWHM ΔV of the assumed line profile, and the isotopic abundance ratio [CO]/[^{13}CO]; it is insensitive to the excitation temperature in ^{13}CO. The regions spanned by the model curve for plausible variations of T_{ex}(CO) and ΔV in Cepheus are shown in Figs. 7a and 7b, respectively. The selected range of ± 1.4 K in T_{ex} corresponds to the rms dispersion of the CO temperature distribution found in the cloud (see Fig. 4a and Table 1). The interval of ± 0.7 km/s in ΔV represents the measured velocity dispersion from line to line. Hence, it seems unlikely that

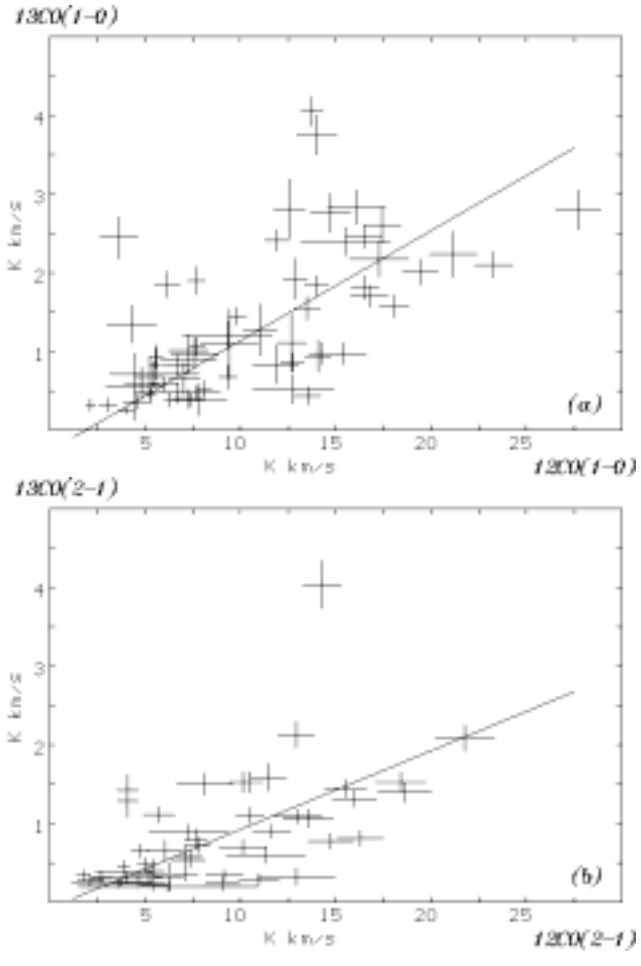

Fig. 6. Correlations between velocity-integrated intensities from the two isotopes of CO, $W(^{13}\mathrm{CO})$ versus $W(^{12}\mathrm{CO})$, in the $1 \rightarrow 0$ **a)** and $2 \rightarrow 1$ **b)** transitions

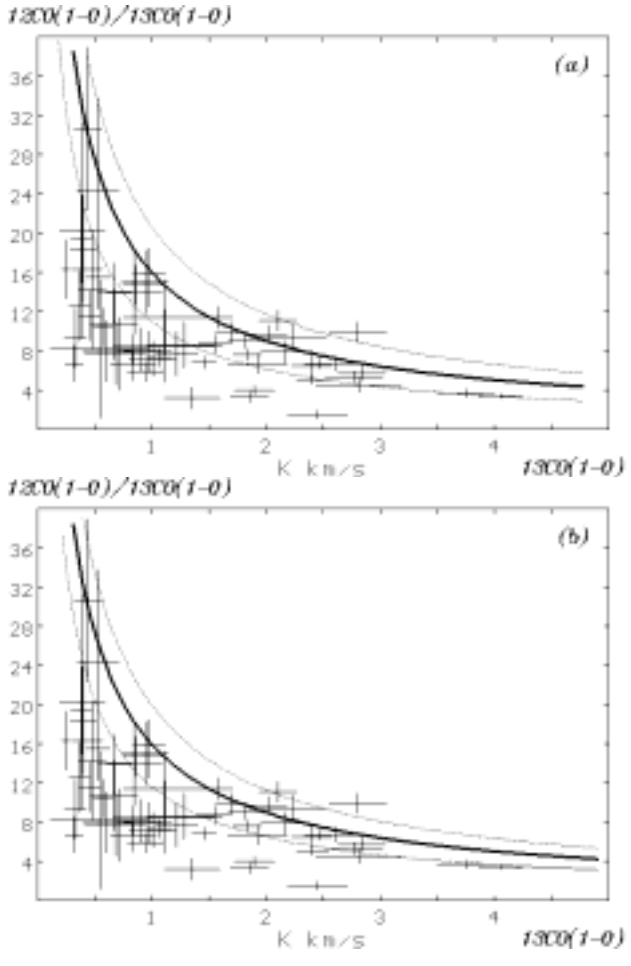

Fig. 7. Observed $W(^{12}\mathrm{CO})/W(^{13}\mathrm{CO})$ ratios as a function of $W(^{13}\mathrm{CO})$ in the $1 \rightarrow 0$ transition. The LTE model curve (thick line) is given for a line width of 2.1 km/s and an excitation temperature of 7.0 K in CO. The thin lines correspond to variations of ± 1.4 K in temperature **a)** and ± 0.7 km/s in line width **b)**

the large scatter observed in the $W(^{12}\mathrm{CO})/W(^{13}\mathrm{CO})$ ratios be caused by variations in the lines width or in CO excitation temperature. In particular, unrealistically cold temperatures or narrow lines would be required to account for the lowest ratios recorded at low or medium $W(^{13}\mathrm{CO})$. These points have been checked individually to be inconsistent with the modelled $W(^{12}\mathrm{CO})/W(^{13}\mathrm{CO})$ ratio expected from their particular temperature and line width. Only one point could be reconciled with the model. In addition, these points have "normal" excitation temperatures in ^{13}CO, close to the mean.

The $W(^{12}\mathrm{CO})/W(^{13}\mathrm{CO})$ ratios in the $2-1$ transition have also been studied at the full resolution of the POM-2 telescope, i.e. $2.3'$ or 0.2 pc locally, to check for possible beam dilution effects. The measured ratios and intensities at $2.3'$ are totally consistent with those presented in Fig. 8 at the reduced resolution of $8.7'$, i.e. 0.8 pc in the cloud. Beam dilution in ^{13}CO cannot explain the lowest $W(^{12}\mathrm{CO})/W(^{13}\mathrm{CO})$ ratios which, on the contrary, require enhanced ^{13}CO emission. One could, however, imagine clumps of gas, unresolved both in CO and ^{13}CO, and dense enough to exhibit low $W(^{12}\mathrm{CO})/W(^{13}\mathrm{CO})$ ratios (hardly sensitive to beam dilution). In Figs. 7 or 8, these points would appear as simply "shifted" to abnormally low $W(^{13}\mathrm{CO})$ intensity. Yet the consistency between the $8.7'$ and $2.3'$ data rules out this possibility.

In conclusion, the observed fluctuations in the $W(^{12}\mathrm{CO})/W(^{13}\mathrm{CO})$ ratio are likely to be due to ^{13}CO abundance variations along the line of sight. The isotopic ratio $[\mathrm{CO}]/[^{13}\mathrm{CO}]$ must be lowered to values between 4 and 10 for the model curve to reach these points. The lowest $W(^{12}\mathrm{CO})/W(^{13}\mathrm{CO})$ ratios recorded may be explained by isotopic fractionation in a low density and cold (< 15 K) ambient gas. Fractionation would be particularly active in the extended envelope of Cepheus where the temperature is low and visual extinction amounts only to ~ 0.5 mag (Lebrun 1986), implying that much of the carbon must be in the form of C^+. Observations of C^+

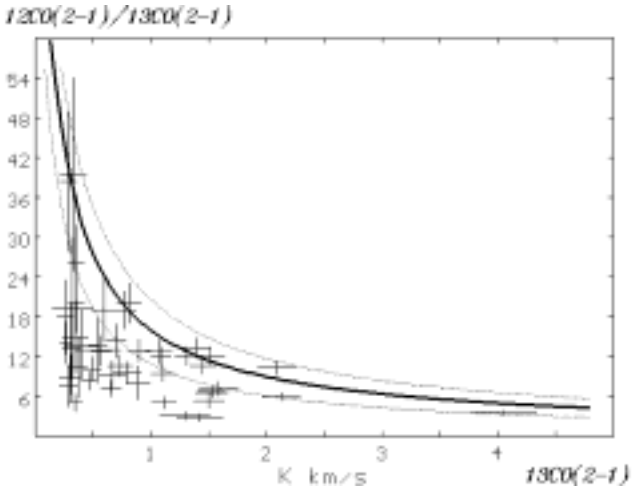

Fig. 8. Observed $W(^{12}\mathrm{CO})/W(^{13}\mathrm{CO})$ ratios as a function of $W(^{13}\mathrm{CO})$ in the $2 \rightarrow 1$ transition. The LTE model curve (thick line) is given for a line width of 2.1 km/s and an excitation temperature of 7.0 K in CO. The thin lines correspond to variations of ± 1.4 K in temperature

emission at 158 μ would be highly desirable to check this effect.

These competing effects introduce a large uncertainty in the "mean" $W(^{12}\mathrm{CO})/W(^{13}\mathrm{CO})$ value obtained for a cloud and may be responsible for the differences observed between Cepheus and other clouds. Among the translucent and high-latitude clouds the ratios range from 3 to 29 around a mean value of about 10 (van Dishoeck et al. 1991). Variations by a factor of 4 occur in the Orion A data of Castets et al. (1990). Observing the fluctuations and dependence of the $W(^{12}\mathrm{CO})/W(^{13}\mathrm{CO})$ ratio with $W(^{13}\mathrm{CO})$ or extinction in a variety of other clouds would give valuable constraints on the theoretical modelling of the photodissociation and fractionation processes in the outer layers of clouds. As a drawback, the intrinsic scatter introduces a large uncertainty in the H_2 mass derivation from ^{13}CO observations.

4. Conclusions

The eastern Cepheus cloud, a nearby translucent and diffuse molecular cloud of $\sim 10^4\ M_\odot$, has been fully mapped in CO($1 \rightarrow 0$). A selection of positions has also been sampled at the same resolution of 0.8 pc in CO($2 \rightarrow 1$), ^{13}CO($1 \rightarrow 0$), and ^{13}CO($2 \rightarrow 1$) to cover the full brightness range of the cloud. The radiative transfer of the lines, under LTE or LVG assumptions, imply low excitation temperatures of $5-11$ K in CO and $4-8$ K in ^{13}CO. The optical depth in CO is moderate ($\tau_{1-0} < 3$ and $\tau_{2-1} < 4$) for CO column-densities up to $\sim 4\ 10^{16}$ cm^{-2} and the cloud is optically thin to ^{13}CO emission up to $\sim 6\ 10^{15}$ cm^{-2}. For both isotopes, these conditions correspond to fairly constant $W_{2\rightarrow1}/W_{1\rightarrow0}$ ratios, as observed over the cloud.

The $W(^{12}\mathrm{CO})/W(^{13}\mathrm{CO})$ ratios have been found to decrease with $W(^{13}\mathrm{CO})$ because of the rapid saturation of the CO lines. Significant fluctuations of the ratios about this relation have also been observed which are comparable to the variations in $W(^{12}\mathrm{CO})/W(^{13}\mathrm{CO})$ or in $N(^{13}\mathrm{CO})/A_V$ reported in two other dark clouds, HCL 2 and IC 5146 on similar linear scales (0.2 pc). Together they indicate that large fluctuations in ^{13}CO abundance or excitation, by a factor up to 4, occur in the cloud envelopes. The distribution of line widths or CO excitation temperatures measured in Cepheus cannot account for the scatter in the $W(^{12}\mathrm{CO})/W(^{13}\mathrm{CO})$ ratios. The excitation conditions of the ^{13}CO molecules are also quite stable and beam dilution of dense clumps is not supported by the $2.3'$ data. So, the large fluctuations in ^{13}CO intensity more likely reflect abundance variations along the line of sight. Isotopic fractionation in the cold environment of Cepheus may easily enhance the ^{13}CO density locally. Detailed observations of the ^{13}CO fluctuations and of C^+ lines would provide important clues to the photodissociation and fractionation processes in the molecular cloud envelopes.

Acknowledgements. G.P.R. and I.A.G. wish to thank Tom Dame and Sam Palmer for their support and assistance during the observations, Alain Castets for lending us his LVG program, and the referee for his helpful remarks.

References

Boden K.-P., Heithausen A., 1993, A&A 268, 255
Bronfman L., et al., 1988, ApJ 324, 248
Castets A., et al., 1990, A&A 234, 469
Castor J.I., 1970, MNRAS 149, 111
Cernicharo J., Guélin M., 1987, A&A 176, 299
Dickman R.L., 1978, ApJS 37, 407
Digel S.W., Grenier I.A., Heithausen A., Hunter S.D., Thaddeus P., 1996, ApJ 463, 609
van Dishoeck E.F., Black J.H., Phillips T.G., Gredel R., 1991, ApJ 366, 141
Flower D.R., Launay J.M., 1985, MNRAS 214, 271
Green S., Thaddeus P., 1976, ApJ 205, 766
Grenier I.A., Lebrun F., Arnaud M., Dame T.M., Thaddeus P., 1989, ApJ 347, 231
Kutner M.L., 1978, ApJ 19, L81
Lada C.L., Lada E.A., Clemens D.P., Bally J., 1994, ApJ 429, 694
Langer W.D., Wilson R.W., Goldsmith P.F., Beichman C.A., 1989, ApJ 337, 355
Lebrun F., 1986, ApJ 306, 16
Lequeux J., et al., 1994, A&A 292, 371
Robert C., Pagani L., 1993, A&A 271, 282
Sakomoto S., et al., 1994, ApJ 425, 641
Sanders D.B., et al., 1993, in Back to the Galaxy, Holt & Verter (eds.). New York: AIP, p. 311
Sato F., Fukui Y., 1989, ApJ 343, 773
Sobolev V.V., 1960, Moving Envelopes of Stars. Cambridge: Harvard University Press
Strong A.W., 1985, A&A 150, 273
Wilson T.L., Rood R.T., 1994, ARA&A 32, 191